

Magnetism and superconductivity in mixed-dimensional periodic Anderson model for UTe_2

Ryuji Hakuno,^{1,*} Kosuke Nogaki,¹ and Youichi Yanase¹

¹*Department of Physics, Graduate School of Science, Kyoto University, Kyoto 606-8502, Japan*

(Dated: June 2, 2023)

UTe_2 is a strong candidate for a topological spin-triplet superconductor, and it is considered that the interplay of magnetic fluctuation and superconductivity is essential for the origin of the superconductivity. Despite various experiments suggesting ferromagnetic criticality, neutron scattering measurements observed only antiferromagnetic fluctuation and called for theories of spin-triplet superconductivity near the antiferromagnetic quantum critical point. We construct a periodic Anderson model with one-dimensional conduction electrons and two- or three-dimensional f -electrons, reminiscent of the band structure of UTe_2 , and show that ferromagnetic and antiferromagnetic fluctuations are reproduced depending on the Fermi surface of f electrons. These magnetic fluctuations cooperatively stabilize spin-triplet p -wave superconductivity. We also study hybridization dependence as a possible origin of pressure-induced superconducting phases and find that moderately large hybridization drastically changes the antiferromagnetic wave vector and stabilizes d -wave superconductivity.

Introduction. — Spin-triplet superconductivity is an exotic quantum condensed state of matter. Interest in spin-triplet superconductors is growing as they are platforms of multi-component superconductivity, bulk topological superconductivity [1–4], and superconducting spintronics [5]. Since the discovery of superconductivity [6], UTe_2 has been considered to be a spin-triplet superconductor, and intensive studies have been devoted to clarifying the superconducting states in UTe_2 [7]. One of the authors previously proposed the existence of topological superconductivity in UTe_2 [8]. However, topological indices and the presence/absence of Majorana fermions depend on the symmetry of the superconducting gap function and the topology of Fermi surfaces. Therefore, a thorough investigation of the nature of the superconductivity and the pairing mechanism is highly desirable.

In early studies, the ferromagnetic quantum critical fluctuation has been indicated [6, 9, 10] and considered to be a glue of spin-triplet Cooper pairs. On the other hand, the neutron scattering experiments detected antiferromagnetic fluctuation [11–14] with the wave vector around $\mathbf{q} \simeq (0, \pi, 0)$ and called for a search for spin-triplet superconductivity arising from antiferromagnetic fluctuation. To study the relationship between magnetic fluctuation and superconductivity, information on the electron band structure is indispensable [15]. An ARPES experiment [16] observed quasi-two-dimensional Fermi surfaces consistent with the LDA+ U [8] and LDA+DMFT calculations [16, 17] for a large Coulomb interaction. Indication of a three-dimensional Fermi surface was also reported [16], but it is under debate [18]. Recent development in crystal growth [19] enabled quantum oscillation measurements [20–23], which precisely detected quasi-two-dimensional Fermi surfaces. The presence or absence of a three-dimensional Fermi surface is still controversial since it is detected only in high fields [22].

Typical uranium-based heavy-fermion superconductors, such as UCoGe and URhGe , exhibit changes in the nature of superconductivity when subjected to pressure [24]. More interestingly, application of pressure to UTe_2 revealed the presence of multiple superconducting phases [25–32]. This experiment suggests that pressure changes the electronic state and

superconductivity. Therefore, theoretical studies revealing intimate relations between electronic states, magnetic fluctuation, and superconductivity have been awaited.

Inspired by the experimental studies on magnetic fluctuation and band structure in UTe_2 , we theoretically investigate Fermi surfaces, magnetic fluctuation, and superconductivity in UTe_2 . Although several microscopic models were analyzed for UTe_2 [15, 33–38], a model reproducing antiferromagnetic fluctuation, Fermi surfaces, and spin-triplet superconductivity was not reported and is highly awaited. In this Letter, we propose a mixed-dimensional periodic Anderson model (PAM) consistent with the band structure calculations [8, 16, 17, 34] and reveal antiferromagnetic fluctuation and spin-triplet superconductivity coherently.

Model and method. — We construct a mixed-dimensional PAM. With a tight-binding model for f , d , and p electrons as a non-interacting part H_0 , the model is given by $H = H_0 + H_1$, where

$$H_0 = H_f + H_d + H_p + H_{fd} + H_{fp} + H_{dp}, \quad (1)$$

$$H_m = \sum_{\mathbf{k}\sigma} (\varepsilon_m(\mathbf{k}) - \mu) a_{m\mathbf{k}\sigma}^\dagger a_{m\mathbf{k}\sigma} \quad (m = f, d, p), \quad (2)$$

$$H_{ml} = \sum_{\mathbf{k}\sigma} V_{ml} a_{m\mathbf{k}\sigma}^\dagger a_{l\mathbf{k}\sigma} + \text{h.c.} \quad (ml = fd, fp, dp), \quad (3)$$

and $H_1 = U \sum_j n_{fj\uparrow} n_{fj\downarrow}$ is the on-site Coulomb interaction of f electrons. The mixed-dimensional property of the model is represented in the kinetic energies,

$$\varepsilon_f(\mathbf{k}) = -2t_{fx} \cos k_x - 2t_{fy} \cos k_y + 2t_{fz}(\cos k_z + 1) + \Delta_f, \quad (4)$$

$$\varepsilon_d(\mathbf{k}) = -2t_{dx} \cos k_x - 2t_{dy} \cos k_y + \Delta_d, \quad (5)$$

$$\varepsilon_p(\mathbf{k}) = 2t_{px} \cos k_x + 2t_{py} \cos k_y + \Delta_p. \quad (6)$$

Here, we assume quasi-one-dimensional conduction electrons in accordance with the band structure of UTe_2 [8, 16, 17]. In UTe_2 , the d and p electrons mainly conduct along the a and b -axis, respectively, corresponding to $t_{dx} \gg t_{dy}$ and $t_{px} \ll t_{py}$. We also assume three-dimensional f electrons with comparable hopping integrals t_{fx} , t_{fy} , and t_{fz} . Thus, conduction

electrons and f electrons have nonequivalent dimensionality, and thus, we call the Hamiltonian the 1+3-dimensional PAM. The 1+2-dimensional PAM can also be constructed by simply setting $t_{fz} = 0$. The results of the 1+2-dimensional model are shown in Supplemental Materials for comparison [39].

The crystal fields are denoted by $\Delta_{p,d,f}$, and we adopt momentum-independent hybridization terms for simplicity. Later, we show that the f -electron level Δ_f and the hybridization with p electrons V_{fp} are control parameters of the model. We set $V_{fp} = 0.05$ unless mentioned otherwise. In the following discussions, we fix the other parameters $(t_{fx}, t_{fy}, t_{fz}, t_{dx}, t_{dy}, \Delta_d, t_{px}, t_{py}, \Delta_p, V_{fd}, V_{dp}, \mu) = (0.08, 0.035, 0.1, 0.5, 0, 0, 0, 1, 0, 0.05, 0.05, -0.1)$ and the temperature $T = 0.01$.

The non-interacting Green function is defined as $\hat{G}(k) = (i\omega_n \hat{I} - \hat{H}_0)^{-1}$, where $k = (\mathbf{k}, i\omega_n)$, $\omega_n = (2n + 1)\pi T$ are fermionic Matsubara frequencies, and \hat{I} is the identity matrix. The spin and charge susceptibilities are evaluated by the random phase approximation (RPA) as

$$\chi_s(q) = \frac{\chi^0(q)}{1 - U\chi^0(q)}, \quad \chi_c(q) = \frac{\chi^0(q)}{1 + U\chi^0(q)}, \quad (7)$$

with the bare susceptibility

$$\chi^0(q) = -\frac{T}{N} \sum_k G_f(k+q)G_f(k). \quad (8)$$

Here, $G_f(k)$ is the f -electron's Green function, $q = (\mathbf{q}, i\Omega_m)$, and $\Omega_m = 2m\pi T$ are bosonic Matsubara frequencies. We investigate superconductivity in this model by solving the Éliashberg equation [40] with the effective interactions given by the RPA,

$$V^s(k-k') = U + \frac{3}{2}U^2\chi_s(k-k') - \frac{1}{2}U^2\chi_c(k-k'), \quad (9)$$

$$V^t(k-k') = -\frac{1}{2}U^2\chi_s(k-k') - \frac{1}{2}U^2\chi_c(k-k'), \quad (10)$$

where the subscript s and t represent the spin-singlet and spin-triplet Cooper pairing channel, respectively. The instability of superconductivity is examined by the linearized Éliashberg equation:

$$\lambda\Delta(k) = -\frac{T}{N} \sum_{k'} V(k-k')|G_f(k')|^2\Delta(k'). \quad (11)$$

The superconducting transition temperature is determined by the condition, $\lambda = 1$. In the following, we discuss superconducting states by calculating the eigenvalue λ . The larger λ indicates the higher transition temperature. The numerical calculations are carried out for the $N = 64 \times 64 \times 64$ lattice and the Matsubara frequency cutoff $N_f = 1024$.

Fermi surface. — First, we show Fermi surfaces of the model. Later we see that magnetic fluctuation drastically changes depending on the shape of Fermi surfaces, which is mainly determined by Δ_f and V_{fp} . As shown in Fig. 1,

when we decrease the f -electron level Δ_f , the Lifshitz transitions successively occur. When we set $\Delta_f = 0.13$, two-dimensional rectangular-shaped Fermi surfaces appear as a consequence of the hybridization of one-dimensional p and d electron bands. A considerable weight of f electrons also exists on the two-dimensional Fermi surfaces owing to the c - f hybridization. A small three-dimensional Fermi surface is present when we decrease the f -electron level as $\Delta_f = 0.08$. By further decreasing Δ_f , the three-dimensional Fermi surface is expanded and connected with the two-dimensional Fermi surfaces (see Fig. 1 for $\Delta_f = 0.038$). A similar change in Fermi surfaces was reported in the band structure calculations for UTe_2 . The LDA+ U and LDA+DMFT calculations for a large Coulomb interaction concluded two-dimensional Fermi surfaces similar to our model for $\Delta_f = 0.13$ [8, 16, 17], while the LDA+ U calculation for an intermediate Coulomb interaction obtained mixed-dimensional Fermi surfaces as reproduced in our model for $\Delta_f = 0.038$ [8]. Thus, the parameter Δ_f in our model may correspond to the interaction parameter of UTe_2 .

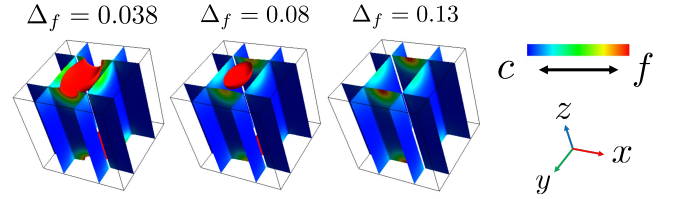


FIG. 1. Fermi surfaces of the mixed-dimensional PAM in Eq. (1). We set $V_{fp} = 0.05$ and vary Δ_f from 0.038 to 0.13. The weight of f electrons is illustrated in red, while the conduction electrons in blue.

In heavy-fermion systems, quantum phase transitions are often tunable by the applied pressure, which has been interpreted as an increase in hybridization. The following results in our model are also sensitive to the hybridization parameter V_{fp} , which affects the shape of the three-dimensional Fermi surface rather than its size. We show the Fermi surfaces for various V_{fp} in Fig. 2. Interestingly, the nesting property changes with V_{fp} , as illustrated in the figure.

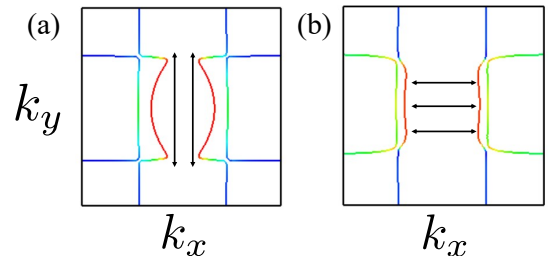


FIG. 2. Fermi surfaces on the $k_z = \pi$ plane for $\Delta_f = 0.05$. (a) $V_{fp} = 0.05$ and (b) $V_{fp} = 0.26$. The weight of f electrons is shown by color as in Fig. 1, and nesting vectors are illustrated by arrows.

Spin susceptibility. — Second, we discuss magnetic fluctuation. Our mixed-dimensional PAM shows ferromagnetic

fluctuation, antiferromagnetic fluctuation, and their coexistence depending on the parameters discussed above. Antiferromagnetic fluctuation is dominant for the f -electron level Δ_f ranging from 0.038 to 0.054, while ferromagnetic fluctuation is dominant for Δ_f from 0.055 to 0.13. To focus on the parameter dependence, we set the Coulomb interaction so that the Stoner factor is $\max U\chi^0(q) = 0.98$. Magnetic susceptibility on the $q_z = 0$ plane is shown in Fig. 3.

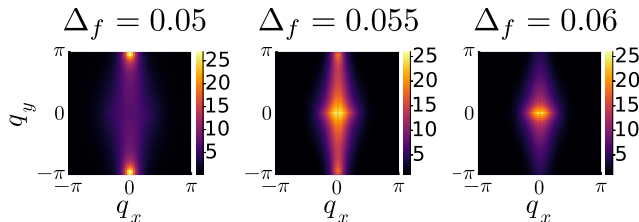


FIG. 3. Static spin susceptibility $\chi_s(\mathbf{q}) \equiv \chi_s(\mathbf{q}, i\Omega_m = 0)$ on the $q_z = 0$ plane for various f -electron levels, Δ_f .

In the result for $\Delta_f = 0.05$, we see antiferromagnetic fluctuation with the wave vector around $\mathbf{q} = (0, \pi, 0)$, consistent with the neutron scattering experiments [11, 12]. Thus, antiferromagnetic fluctuation in UTe_2 can be explained by the nesting vector of Fermi surfaces with substantial f -electrons, as shown in Fig. 2(a). On the other hand, when we slightly increase the f -electron level as $\Delta_f = 0.055$, ferromagnetic fluctuation with the wave vector $\mathbf{q} = 0$ becomes dominant and coexists with antiferromagnetic fluctuation. Ferromagnetic fluctuation naturally arises from the three-dimensional property of f electrons. Thus, (anti)ferromagnetic fluctuations are sensitive to the parameters, and they can coexist. This finding may be consistent with the fact that UTe_2 has been considered to be a nearly ferromagnetic system [6, 7, 9, 10, 41] and coexisting ferro- and antiferromagnetic fluctuations were reported [17, 42].

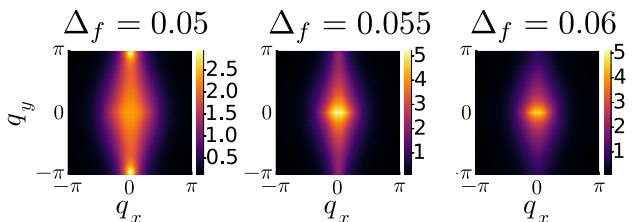


FIG. 4. Spin susceptibility integrated along the q_z direction, defined by $\chi_z^{2d}(q_x, q_y) \equiv \int \chi_s(\mathbf{q}) dq_z$.

In our model, magnetic susceptibility always shows maximum on the $q_z = 0$ plane. To get information on magnetic fluctuation away from $q_z = 0$, Fig. 4 shows the integration of spin susceptibility with respect to q_z . Even for $\Delta_f = 0.05$ resulting in dominant antiferromagnetic fluctuation, magnetic fluctuation has substantial weight around $(q_x, q_y) = (0, 0)$, indicating two-dimensional ferromagnetic fluctuation. Because two-dimensional fluctuation generally favors superconductiv-

ity [40], ferromagnetic correlation is expected to play an important role in superconductivity.

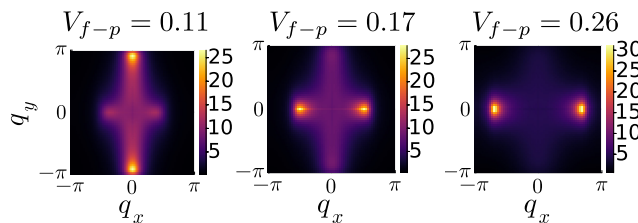


FIG. 5. Spin susceptibility on the $q_z = 0$ plane for various hybridization parameters, V_{f-p} . We fix the f -electron level $\Delta_f = 0.05$.

As shown above, the mixed-dimensional PAM reproduces both ferromagnetic and antiferromagnetic fluctuations that are considered to exist in UTe_2 . The three-dimensional f electrons are crucially important for magnetic fluctuations [39]. Furthermore, the model can reproduce a theoretical study for UTe_2 under pressures [33], in which antiferromagnetic fluctuation with the wave vector $\mathbf{q} \simeq (\pi, 0, 0)$ develops by increasing c - f hybridization. Figure 5 shows the spin susceptibility in the mixed-dimensional PAM for strong hybridization. We see that the wave vector of antiferromagnetic fluctuation changes from $\mathbf{q} \simeq (0, \pi, 0)$ to $\mathbf{q} \simeq (\pi, 0, 0)$. This is because the strong hybridization changes the Fermi surfaces and results in better nesting along the x -direction as shown in Fig. 2(b).

Superconductivity. — Next, we examine superconductivity mediated by magnetic fluctuations. In particular, we focus on the relation between the wave vector of magnetic fluctuation and the symmetry of superconductivity.

TABLE I. Irreducible representations and basis functions of the D_{2h} point group.

IR(D_{2h})	A_g	B_{1g}	B_{2g}	B_{3g}	A_u	B_{1u}	B_{2u}	B_{3u}
Basis function	1	$k_x k_y$	$k_x k_z$	$k_y k_z$	$k_x k_y k_z$	k_z	k_y	k_x

For this purpose, we solve the linearized Éliashberg equation for all the irreducible representations of the D_{2h} point group. Note that the model in this study does not include a spin-orbit coupling. Therefore, we classify the gap function $\Delta(k)$ by the representation without a spin degree of freedom. Table II shows the list of irreducible representations and basis functions. In this classification, the B_{1u} , B_{2u} , and B_{3u} representations correspond to the p -wave superconductivity while the A_u representation does the f -wave superconductivity. The other representations indicate spin-singlet superconductivity with either s -wave or d -wave symmetry.

First, we show Fig. 6 for the Δ_f dependence of eigenvalues of Éliashberg equation. We see that spin-triplet p -wave superconductivity of B_{1u} and B_{3u} representations is stable over a wide range of parameters. In particular, the p -wave superconductivity is stable even around $\Delta_f = 0.05$ where antiferromagnetic fluctuation is dominant. This is because ferro-

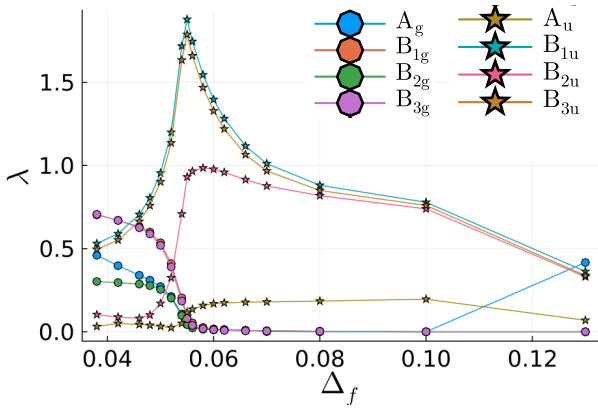


FIG. 6. Eigenvalues of Éliashberg equation as a function of the f -electron level Δ_f . The maximum values for each irreducible representation are shown. Spin-triplet superconductivity and spin-singlet superconductivity are plotted by stars and circles, respectively.

magnetic fluctuation and antiferromagnetic fluctuation cooperatively stabilize the p -wave superconductivity. Indeed, the p -wave superconductivity is most stable when the two fluctuations coexist, as the eigenvalue λ shows the maximum around $\Delta_f = 0.055$.

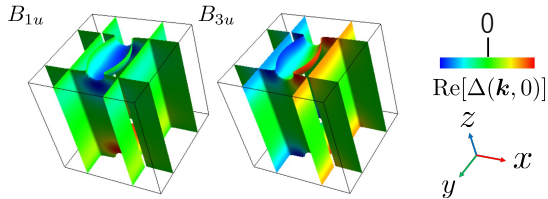


FIG. 7. The gap functions of B_{1u} and B_{3u} representations on the Fermi surfaces. The color represents the real part of the gap function.

The antiferromagnetic fluctuation can favor spin-triplet superconductivity when the gap function has the same sign between the Fermi momentum connected by the nesting vector [40]. This condition is indeed satisfied for the B_{1u} and B_{3u} representations. Figure 7 shows the gap functions on the Fermi surfaces for $\Delta_f = 0.05$, where the static gap function is defined as

$$\Delta(\mathbf{k}, 0) \equiv \frac{\Delta(\mathbf{k}, i\pi T) + \Delta(\mathbf{k}, -i\pi T)}{2}. \quad (12)$$

Antiferromagnetic fluctuation with $\mathbf{q} = (0, \pi, 0)$ acts as an attractive force for the B_{1u} and B_{3u} representations because the gap functions on the Fermi surface do not change the sign for the magnetic scattering. However, it gives a repulsive interaction for the B_{2u} representation, and thus the B_{2u} state is suppressed. For $\Delta_f > 0.08$, all the p -wave superconducting states are nearly degenerate, because the antiferromagnetic fluctuation is negligible.

Next, we show the hybridization V_{fp} dependence of superconductivity. In Fig. 8, we see that stable superconducting states are the spin-triplet B_{1u} and B_{3u} states for small

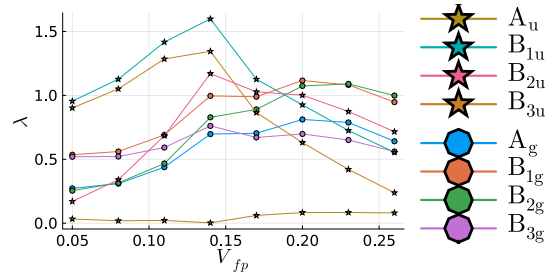


FIG. 8. The hybridization dependence of superconductivity, indicated by the eigenvalues λ of Éliashberg equation. We set $\Delta_f = 0.05$.

V_{fp} , while the spin-singlet B_{1g} and B_{2g} states are stable for large V_{fp} . This can be regarded as a parity transition of superconductivity, where the symmetry of superconductivity changes from odd-parity to even-parity by increasing the magnitude of hybridization. Accompanied by the development of antiferromagnetic fluctuation with $\mathbf{q} \parallel \hat{x}$, the spin-singlet superconductivity of the B_{1g} and B_{2g} representations is favored. The hybridization dependence obtained above is qualitatively consistent with the previous study [33], where the extended s -wave state is stable instead of the d -wave one. Since the hybridization is expected to be enhanced by pressure in heavy-fermion systems, the parity transition may correspond to the multiple superconducting phases of UTe_2 under pressures [7, 25]. However, the pressure changes various parameters including the f -electron level and Coulomb interaction, and therefore, further verification based on first-principles calculations combined with experiments is desirable.

Summary and discussion. — In this Letter, we have proposed the 1+3-dimensional PAM as a minimal model for Fermi surfaces, magnetic fluctuation, and superconductivity in UTe_2 . The model reproduces the antiferromagnetic and ferromagnetic fluctuations which have been indicated by experiments. The spin-triplet superconductivity is cooperatively stabilized by these magnetic fluctuations. We emphasize that the spin-triplet p -wave superconductivity can coexist with antiferromagnetic fluctuation in contrast to the common belief. This is a characteristic property of the 1+3-dimensional model, as we find that spin-triplet superconductivity and antiferromagnetic fluctuation are exclusive in the 1+2-dimensional PAM [39].

We can extend the mixed-dimensional PAM to include spin-orbit coupling, magnetic field, and multiple orbitals and sublattices. Thus, we expect that the model will be the basis of further theoretical studies for UTe_2 . Our calculation indicates the k_x and k_z orbital components of order parameters. However, the spin-triplet superconducting states are degenerate because of the spin component in our model. Spin-orbit coupling and magnetic fields break the spin $\text{SU}(2)$ symmetry and play essential roles in determining the spin component. Thus, calculations containing these effects are desirable in the future to identify the multiple superconducting phases under pressures [7, 25–32] and/or magnetic fields [7, 43–47]. Recently,

development in the high-purity crystal growth [19] makes a second era in experiments of UTe_2 . For instance, the quantum oscillation was detected [20–23], and the thermal conductivity [48] and NMR Knight shift [49] show behaviors consistent with the order parameter $\mathbf{d} = k_x \hat{x} + k_y \hat{y} + k_z \hat{z}$, similar to the B-phase of ^3He [50]. The order parameter contains the k_x and k_z orbital components consistent with our results and realizes strong (weak) topological superconductivity in the presence (absence) of a three-dimensional Fermi surface [8, 51].

We appreciate helpful discussions with J. Ishizuka, D. Aoki, J.-P. Brison, K. Ishida, G. Knebel, Y. Matsuda, S. Suet-sugu, Y. Tokiwa, and Y. Tokunaga. We use FermiSurfer to describe the Fermi surfaces in this paper [52]. This work was supported by JSPS KAKENHI (Grant Nos. JP21K18145, JP22H01181, JP22H04933).

* hakuno.ryuji.46v@st.kyoto-u.ac.jp

- [1] A. P. Schnyder, S. Ryu, A. Furusaki, and A. W. W. Ludwig, *Phys. Rev. B* **78**, 195125 (2008).
- [2] M. Sato, *Phys. Rev. B* **81**, 220504 (2010).
- [3] L. Fu and E. Berg, *Phys. Rev. Lett.* **105**, 097001 (2010).
- [4] M. Sato and S. Fujimoto, *Journal of the Physical Society of Japan* **85**, 072001 (2016), <https://doi.org/10.7566/JPSJ.85.072001>.
- [5] J. Linder and J. W. A. Robinson, *Nature Physics* **11**, 307 (2015).
- [6] S. Ran, C. Eckberg, Q. P. Ding, Y. Furukawa, T. Metz, S. R. Saha, I. L. Liu, M. Zic, H. Kim, J. Paglione, and N. P. Butch, *Science* **365**, 684 (2019).
- [7] D. Aoki, J.-P. Brison, J. Flouquet, K. Ishida, G. Knebel, Y. Tokunaga, and Y. Yanase, *Journal of Physics: Condensed Matter* **34**, 243002 (2022).
- [8] J. Ishizuka, S. Sumita, A. Daido, and Y. Yanase, *Phys. Rev. Lett.* **123**, 217001 (2019).
- [9] S. Sundar, S. Gheidi, K. Akintola, A. M. Côté, S. R. Dunsiger, S. Ran, N. P. Butch, S. R. Saha, J. Paglione, and J. E. Sonier, *Phys. Rev. B* **100**, 140502(R) (2019).
- [10] Y. Tokunaga, H. Sakai, S. Kambe, T. Hattori, N. Higa, G. Nakamine, S. Kitagawa, K. Ishida, A. Nakamura, Y. Shimizu, Y. Homma, D. X. Li, F. Honda, and D. Aoki, *J. Phys. Soc. Jpn.* **88**, 073701 (2019).
- [11] C. Duan, K. Sasmal, M. B. Maple, A. Podlesnyak, J.-X. Zhu, Q. Si, and P. Dai, *Phys. Rev. Lett.* **125**, 237003 (2020).
- [12] W. Knafo, G. Knebel, P. Steffens, K. Kaneko, A. Rosuel, J.-P. Brison, J. Flouquet, D. Aoki, G. Lapertot, and S. Raymond, *Phys. Rev. B* **104**, L100409 (2021).
- [13] C. Duan, R. E. Baumbach, A. Podlesnyak, Y. Deng, C. Moir, A. J. Breindel, M. B. Maple, E. M. Nica, Q. Si, and P. Dai, *Nature* **600**, 636 (2021).
- [14] S. Raymond, W. Knafo, G. Knebel, K. Kaneko, J.-P. Brison, J. Flouquet, D. Aoki, and G. Lapertot, *J. Phys. Soc. Jpn.* **90**, 113706 (2021).
- [15] A. Kreisel, Y. Quan, and P. J. Hirschfeld, *Phys. Rev. B* **105**, 104507 (2022).
- [16] L. Miao, S. Liu, Y. Xu, E. C. Kotta, C.-J. Kang, S. Ran, J. Paglione, G. Kotliar, N. P. Butch, J. D. Denlinger, and L. A. Wray, *Phys. Rev. Lett.* **124**, 076401 (2020).
- [17] Y. Xu, Y. Sheng, and Y.-f. Yang, *Phys. Rev. Lett.* **123**, 217002 (2019).
- [18] S.-i. Fujimori, I. Kawasaki, Y. Takeda, H. Yamagami, A. Nakamura, Y. Homma, and D. Aoki, *Journal of the Physical Society of Japan* **90**, 015002 (2021), <https://doi.org/10.7566/JPSJ.90.015002>.
- [19] H. Sakai, P. Opletal, Y. Tokiwa, E. Yamamoto, Y. Tokunaga, S. Kambe, and Y. Haga, *Phys. Rev. Mater.* **6**, 073401 (2022).
- [20] D. Aoki, H. Sakai, P. Opletal, Y. Tokiwa, J. Ishizuka, Y. Yanase, H. Harima, A. Nakamura, D. Li, Y. Homma, Y. Shimizu, G. Knebel, J. Flouquet, and Y. Haga, *Journal of the Physical Society of Japan* **91**, 083704 (2022), <https://doi.org/10.7566/JPSJ.91.083704>.
- [21] A. G. Eaton, T. I. Weinberger, N. J. M. Popiel, Z. Wu, A. J. Hickey, A. Cabala, J. Pospisil, J. Prokleska, T. Haidamak, G. Bastien, P. Opletal, H. Sakai, Y. Haga, R. Nowell, S. M. Benjamin, V. Sechovsky, G. G. Lonzarich, F. M. Grosche, and M. Valiska, “Quasi-2d fermi surface in the anomalous superconductor UTe_2 ,” (2023), [arXiv:2302.04758](https://arxiv.org/abs/2302.04758) [cond-mat.supr-con].
- [22] C. Broyles, Z. Rehfuss, H. Siddiquee, K. Zheng, Y. Le, M. Nikolo, D. Graf, J. Singleton, and S. Ran, “Revealing a 3d fermi surface and electron-hole tunneling in UTe_2 with quantum oscillations,” (2023), [arXiv:2303.09050](https://arxiv.org/abs/2303.09050) [cond-mat.str-el].
- [23] D. Aoki, I. Sheikin, A. McCollam, J. Ishizuka, Y. Yanase, G. Lapertot, J. Flouquet, and G. Knebel, *Journal of the Physical Society of Japan* **92**, 065002 (2023), <https://doi.org/10.7566/JPSJ.92.065002>.
- [24] D. Aoki, K. Ishida, and J. Flouquet, *Journal of the Physical Society of Japan* **88**, 022001 (2019), <https://doi.org/10.7566/JPSJ.88.022001>.
- [25] D. Braithwaite, M. Vališka, G. Knebel, G. Lapertot, J. P. Brison, A. Pourret, M. E. Zhitomirsky, J. Flouquet, F. Honda, and D. Aoki, *Communications Physics* **2**, 1 (2019).
- [26] D. Aoki, F. Honda, G. Knebel, D. Braithwaite, A. Nakamura, D. Li, Y. Homma, Y. Shimizu, Y. J. Sato, J.-P. Brison, and J. Flouquet, *J. Phys. Soc. Jpn.* **89**, 053705 (2020).
- [27] W. C. Lin, D. J. Campbell, S. Ran, I. L. Liu, H. Kim, A. H. Nev- idomskyy, D. Graf, N. P. Butch, and J. Paglione, *npj Quantum Materials* **5**, 1 (2020).
- [28] S. Ran, H. Kim, I. L. Liu, S. R. Saha, I. Hayes, T. Metz, Y. S. Eo, J. Paglione, and N. P. Butch, *Phys. Rev. B* **101**, 140503(R) (2020).
- [29] S. M. Thomas, F. B. Santos, M. H. Christensen, T. Asaba, F. Ronning, J. D. Thompson, E. D. Bauer, R. M. Fernandes, G. Fabbris, and P. F. Rosa, *Sci. Adv.* **6**, eabc8709 (2020).
- [30] G. Knebel, M. Kimata, M. Vališka, F. Honda, D. Li, D. Braithwaite, G. Lapertot, W. Knafo, A. Pourret, Y. J. Sato, Y. Shimizu, T. Kihara, J.-P. Brison, J. Flouquet, and D. Aoki, *J. Phys. Soc. Jpn.* **89**, 053707 (2020).
- [31] D. Aoki, M. Kimata, Y. J. Sato, G. Knebel, F. Honda, A. Nakamura, D. Li, Y. Homma, Y. Shimizu, W. Knafo, D. Braithwaite, M. Vališka, A. Pourret, J.-P. Brison, and J. Flouquet, *Journal of the Physical Society of Japan* **90**, 074705 (2021), <https://doi.org/10.7566/JPSJ.90.074705>.
- [32] P. F. S. Rosa, A. Weiland, S. S. Fender, B. L. Scott, F. Ronning, J. D. Thompson, E. D. Bauer, and S. M. Thomas, *Communications Materials* **3**, 33 (2022).
- [33] J. Ishizuka and Y. Yanase, *Phys. Rev. B* **103**, 094504 (2021).
- [34] T. Shishidou, H. G. Suh, P. M. R. Brydon, M. Weinert, and D. F. Agterberg, *Phys. Rev. B* **103**, 104504 (2021).
- [35] T. Hazra and P. Coleman, *Phys. Rev. Lett.* **130**, 136002 (2023).
- [36] L. Chen, H. Hu, C. Lane, E. M. Nica, J.-X. Zhu, and Q. Si, “Multiorbital spin-triplet pairing and spin resonance in the heavy-fermion superconductor UTe_2 ,” (2021), [arXiv:2112.14750](https://arxiv.org/abs/2112.14750) [cond-mat.supr-con].

- [37] H. C. Choi, S. H. Lee, and B.-J. Yang, “Correlated normal state fermiology and topological superconductivity in ute_2 ,” (2023), [arXiv:2206.04876](https://arxiv.org/abs/2206.04876) [cond-mat.supr-con].
- [38] J. J. Yu, Y. Yu, D. F. Agterberg, and S. Raghu, “Theory of the low- and high-field superconducting phases of ute_2 ,” (2023), [arXiv:2303.02152](https://arxiv.org/abs/2303.02152) [cond-mat.supr-con].
- [39] See Supplemental Materials for the results of the 1+2-dimensional periodic Anderson model.
- [40] Y. Yanase, T. Jujo, T. Nomura, H. Ikeda, T. Hotta, and K. Yamada, *Physics Reports* **387**, 1 (2003).
- [41] H. Fujibayashi, K. Kinjo, G. Nakamine, S. Kitagawa, K. Ishida, Y. Tokunaga, H. Sakai, S. Kambe, A. Nakamura, Y. Shimizu, Y. Homma, D. Li, F. Honda, and D. Aoki, *Journal of the Physical Society of Japan* **92**, 053702 (2023), <https://doi.org/10.7566/JPSJ.92.053702>.
- [42] D. V. Ambika, Q.-P. Ding, K. Rana, C. E. Frank, E. L. Green, S. Ran, N. P. Butch, and Y. Furukawa, *Phys. Rev. B* **105**, L220403 (2022).
- [43] S. Ran, I.-L. Liu, Y. S. Eo, D. J. Campbell, P. M. Neves, W. T. Fuhrman, S. R. Saha, C. Eckberg, H. Kim, D. Graf, F. Balakirev, J. Singleton, J. Paglione, and N. P. Butch, *Nature Physics* **15**, 1250 (2019).
- [44] A. Rosuel, C. Marcenat, G. Knebel, T. Klein, A. Pourret, N. Marquardt, Q. Niu, S. Rousseau, A. Demuer, G. Seyfarth, G. Lapertot, D. Aoki, D. Braithwaite, J. Flouquet, and J. P. Brison, *Phys. Rev. X* **13**, 011022 (2023).
- [45] K. Kinjo, H. Fujibayashi, S. Kitagawa, K. Ishida, Y. Tokunaga, H. Sakai, S. Kambe, A. Nakamura, Y. Shimizu, Y. Homma, D. X. Li, F. Honda, D. Aoki, K. Hiraki, M. Kimata, and T. Sasaki, *Phys. Rev. B* **107**, L060502 (2023).
- [46] Y. Tokiwa, P. Opletal, H. Sakai, K. Kubo, E. Yamamoto, S. Kambe, M. Kimata, S. Awaji, T. Sasaki, D. Aoki, Y. Tokunaga, and Y. Haga, “Stabilization of superconductivity by metamagnetism in an easy-axis magnetic field on ute_2 ,” (2022), [arXiv:2210.11769](https://arxiv.org/abs/2210.11769) [cond-mat.supr-con].
- [47] H. Sakai, Y. Tokiwa, P. Opletal, M. Kimata, S. Awaji, T. Sasaki, D. Aoki, S. Kambe, Y. Tokunaga, and Y. Haga, *Phys. Rev. Lett.* **130**, 196002 (2023).
- [48] S. Suetsugu *et al.*, submitted.
- [49] H. Matsumura, H. Fujibayashi, K. Kinjo, S. Kitagawa, K. Ishida, Y. Tokunaga, H. Sakai, S. Kambe, A. Nakamura, Y. Shimizu, Y. Homma, D. Li, F. Honda, and D. Aoki, “Large reduction in the a -axis knight shift on ute_2 with $t_c = 2.1$ k,” (2023), [arXiv:2305.01200](https://arxiv.org/abs/2305.01200) [cond-mat.supr-con].
- [50] A. J. Leggett, *Rev. Mod. Phys.* **47**, 331 (1975).
- [51] J. Tei, T. Mizushima, and S. Fujimoto, *Phys. Rev. B* **107**, 144517 (2023).
- [52] M. Kawamura, *Computer Physics Communications* **239**, 197 (2019).

Supplemental Materials:
**Magnetism and superconductivity in
 mixed-dimensional periodic Anderson model
 for UTe_2**

1+2-DIMENSIONAL PERIODIC ANDERSON MODEL

We show the results of the 1+2-dimensional periodic Anderson model to compare the model with the 1+3-dimensional periodic Anderson model discussed in the main text. Combining the results of 1+2- and 1+3-dimensional models, we reveal general properties of the mixed-dimensional periodic Anderson model. In the 1+2-dimensional periodic Anderson model, the hopping integral of f electrons along of the k_z direction is taken as zero, $t_{fz} = 0$. The other parameters are the same as the 1+3-dimensional model. We study magnetic fluctuation and superconducting instability by changing the f -electron level Δ_f from 0.05 to 0.13, as we have done for the 1+3-dimensional model in the main text.

First, Fermi surfaces of the 1+2-dimensional periodic Anderson model are shown in Fig. 9. They are equivalent to the Fermi surfaces of the 1+3-dimensional model at $k_z = \pi$.

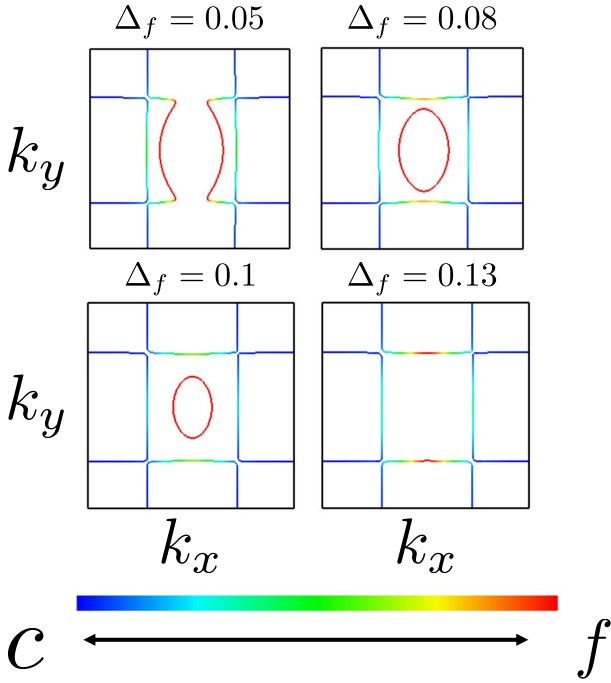


FIG. 9. Fermi surfaces of the 1+2-dimensional periodic Anderson model. The color indicates the weight of f electrons.

Second, we show the spin susceptibility in Fig. 10. We see antiferromagnetic fluctuation with the wave vector $\mathbf{q} = (0, \pi)$ when $\Delta_f = 0.05$, the same as in the 1+3-dimensional model. In the 1+2-dimensional model, ferromagnetic fluctuation is not obtained for Δ_f ranging from 0.05 to 0.07, different from the 1+3-dimensional model where ferromagnetic fluctuation

appears above $\Delta_f = 0.05$. The wave vector of antiferromagnetic fluctuation changes with increasing Δ_f and crossovers to ferromagnetic fluctuation around $\Delta_f = 0.08$. Thus, the region where antiferromagnetic fluctuation dominates is broader than that in the 1+3-dimensional model. This is because the two-dimensional model has better nesting properties than the three-dimensional model and the cylindrical Fermi surface is less likely to show ferromagnetic fluctuation than the spherical Fermi surface.

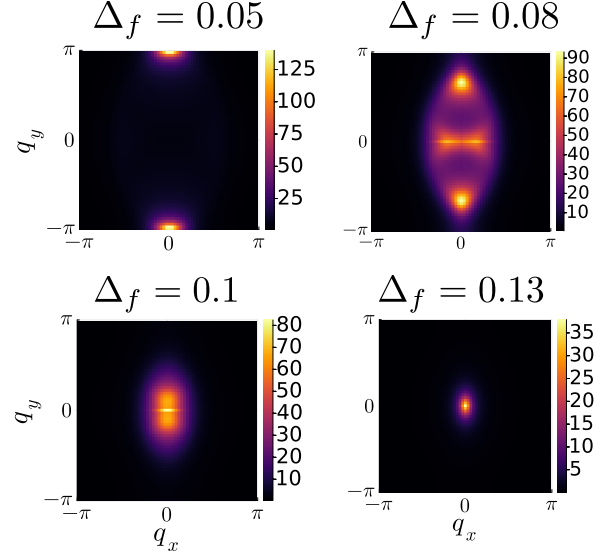


FIG. 10. Static spin susceptibility $\chi_s(\mathbf{q}) \equiv \chi_s(\mathbf{q}, i\Omega_m = 0)$ for various f -electron levels Δ_f .

TABLE II. Irreducible representations and basis functions in the 1+2-dimensional model.

IR(D_{2h})	A_g	B_{1g}	B_{2u}	B_{3u}
Basis function	1	$k_x k_y$	k_y	k_x

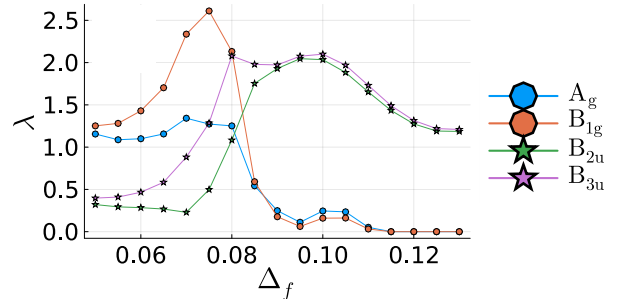


FIG. 11. Eigenvalues of Éliashberg equation for superconductivity in the 1+2-dimensional periodic Anderson model. Δ_f dependence is shown for each irreducible representation of the D_{2h} point group (Table II).

Next, we discuss superconductivity. The gap function in

the 1+2-dimensional model does not have k_z dependence, and therefore, the superconducting states are classified by the irreducible representations in Table II. The eigenvalues of Éliashberg equation as functions of Δ_f are shown in Fig. 11. We see the stable superconducting state changes from the B_{1g} representation to the B_{2u} and B_{3u} representations at around $\Delta_f = 0.08$, associated with antiferromagnetic to ferromagnetic crossover in magnetic fluctuation. For $\Delta_f < 0.08$, the spin-singlet superconducting state of B_{1g} representation is stabilized by antiferromagnetic fluctuation. On the other hand, for $\Delta_f > 0.08$, spin-triplet superconducting states of B_{2u} and B_{3u} representations are stabilized by ferromagnetic fluctuation, and spin-singlet B_{1g} and A_g states are almost suppressed. It is stressed that antiferromagnetic fluctuation and spin-triplet p -wave superconductivity do not coexist in the 1+2-dimensional model, in contrast to the 1+3-dimensional model. The gap function on the Fermi surface for $\Delta_f = 0.05$

is shown in Fig. 12.

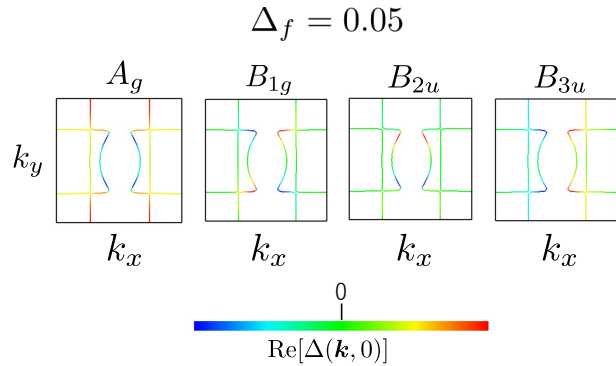


FIG. 12. Superconducting gap function in the 1+2-dimensional periodic Anderson model for $\Delta_f = 0.05$.